

Structural characterization of Au/Cu_{1-x}Mn_xFe₂O₄ catalysts suitable for WGSR

T. M. Petrova*, N. I. Velinov, I. B. Ivanov, T. T. Tabakova,
V. D. Idakiev, I. G. Mitov

Institute of Catalysis, Bulgarian Academy of Sciences, 1113 Sofia, Bulgaria

Received October 12, 2018; Accepted December 04, 2018

The spinel ferrites are known to have many important properties as magnetic, optical, catalytic etc., which provokes the scientific interest. Copper-manganese-iron samples with nominal compositions Cu_{1-x}Mn_xFe₂O₄ (x=0; 0.2; 0.4; 0.6; 0.8 and 1) were prepared by auto-combustion sol-gel method and modification by gold was carried out by deposition-precipitation procedure. Their performance in the water-gas shift reaction (WGSR) was investigated. Structural characteristics of samples were determined by X-Ray diffraction and Mössbauer spectroscopy. Spinel ferrite phase and gold phase were proved in all synthesized samples. In copper-rich composition additional phase of CuO was present. The cation distribution in octahedral and tetrahedral positions in spinel lattice and the presence of superparamagnetic particles were evaluated by Mössbauer spectroscopy. Catalytic activities in the WGSR of studied samples followed the order: Au/Cu_{0.2}Mn_{0.8}Fe₂O₄ ≥ Au/Cu_{0.5}Mn_{0.5}Fe₂O₄ > Au/Cu_{0.8}Mn_{0.2}Fe₂O₄ > Au/CuFe₂O₄ ≥ Au/MnFe₂O₄. Some changes in the phase composition and structure of both gold and spinel ferrite phases were found after WGSR. Full or partial alloying of gold with copper was evidenced. The main samples transformation in reactive atmosphere was partial reduction of the ferrite phase. The result of this reduction was the formation of metallic copper and copper and/or manganese substituted magnetite in mixed copper-manganese containing samples. Simultaneous presence of both phases could be considered as a reason for better catalytic activity of mixed ferrites.

Keywords: copper-manganese ferrites, gold catalysts, Mössbauer spectroscopy, WGSR.

1. INTRODUCTION

Depending on the distribution of divalent and trivalent cations in tetrahedral and octahedral positions, the spinel structure is divided into three groups – normal, inverse and partially inverse. When all divalent cations occupy only tetrahedral positions, the spinels are called normal, inverse – when divalent cations occupy only octahedral sites and partially inverse when divalent ions are distributed in tetrahedral and octahedral positions. Certain fact is that different metal cations have different preferences to occupy tetrahedral and octahedral positions in the structure of spinel [1, 2]. It is also known that cationic distribution affects the functional properties of ferrites such as magnetic, optical, catalytic, etc. [3–10]. This fact provoked the study of the relationship between the structure and the functional properties of spinel ferrites [3–5], [11]. A typical example of catalyst with spinel structure is magnet-

ite (Fe₃O₄), which is the main active phase of the iron-containing catalysts in the high temperature stage of WGSR, which is carried out at 350–450 °C [6].

Various spinel ferrite materials have been successfully synthesized by applying auto-combustion sol-gel technology [12–17]. It has been shown that the conditions of synthesis affect the phase impurities, the crystallinity, and therefore the particle size, the agglomerating ability, which actually reduces the specific surface [12]. However, it has been found that in some cases the multi-component ferrites have better catalytic behaviour than the mono-component ferrite [7–9], [18]. The development of copper-based ferrite catalysts has been a major challenge in recent years [19]. An example of this is copper ferrite, which is an inverse spinel, since the iron atoms are distributed in tetrahedral and octahedral positions, and the copper ions occupy predominantly octahedral positions. In addition, magnetite materials substituted with Cr, Mn, Co, Ni, Cu, Zn and Ce ions have a very simple Fe³⁺ ⇌ Fe²⁺ reducing pair, from which it can be concluded that Cu-containing ferrites are very promising for

* To whom all correspondence should be sent:
E-mail: silberbarren@abv.bg

WGSR applications [20]. In his article, Khan et al. [20], note that the rapid electron exchange between $\text{Fe}^{3+} \rightleftharpoons \text{Fe}^{2+}$ in the Fe_3O_4 is essential for conducting the WGS reaction. It has also been shown that the precious metal catalysts (platinum and gold) have very good catalytic activity in WGSR, and modified by gold oxide exhibits high catalytic activity at low temperature [21].

The aim of the present work is to study structural characteristics of gold modified copper-manganese ferrite catalysts. Object of the investigation are materials with compositions $\text{Au/Cu}_{1-x}\text{Mn}_x\text{Fe}_2\text{O}_4$ ($0 \leq x \leq 1$) before and after catalytic test in WGSR. The correlation between Cu/Mn ratio, catalyst structure, and catalytic activity are also discussed.

2. EXPERIMENTAL

2.1. Synthesis

Copper-manganese-iron samples with nominal compositions $\text{Cu}_{1-x}\text{Mn}_x\text{Fe}_2\text{O}_4$, where $x=0; 0.2; 0.4; 0.6; 0.8$ and 1 were prepared by auto-combustion sol-gel method using the procedure reported in [10]. Shortly, the experimental procedure was as follows: the corresponding stoichiometric amount from the starting nitrate salts $\text{Cu}(\text{NO}_3)_2 \cdot 3\text{H}_2\text{O}$, $\text{Mn}(\text{NO}_3)_2 \cdot 4\text{H}_2\text{O}$ and $\text{Fe}(\text{NO}_3)_3 \cdot 9\text{H}_2\text{O}$ was dissolved in distilled water at room temperature and constant stirring; citric acid was added to the solution in a molar ratio equal to the sum of the metal ions (Cu, Mn, Fe) and stirring was continued at 60°C ; the water was evaporated from the solution by heating and continuous stirring on a magnetic stirrer; the auto-combustion process was performed by heating the samples in an oven at 150°C for 1 hour. The samples were further thermally treated at 300°C .

The modification of ferrite samples by gold (2 wt.%) was carried out by deposition-precipitation method. The ferrite material was suspended in water, and the deposition was performed by simultaneous addition of an aqueous solution of HAuCl_4 and Na_2CO_3 at 60°C and pH 7. The next steps included aging at 60°C for 1 hour, filtering and washing until complete removal of Cl^- ions, drying under vacuum at 80°C and calcination in air at 400°C for 2 hours. The samples were denoted as $\text{Au/Cu}_{1-x}\text{Mn}_x\text{Fe}_2\text{O}_4$.

2.2. Methods of characterization

Powder X-ray diffraction (XRD) analysis was carried out by TUR M62 diffractometer with $\text{Co K}\alpha$ radiation. Phase identification was performed using ICDD-PDF2 Database. The structural characteristics of the studied phases were determined from the experimental XRD profiles by using the

PowderCell-2.4 software [21]. The average crystallites size is determined using the Williamson-Hall method with appropriate corrections for the instrumental broadening. According to the method, the diffraction lines are treated using the Voigt function, which Lorentzian and Gaussian components are used for the elucidation of the average particles size and microstrain, respectively.

The Mössbauer spectra were obtained in air at room temperature (RT) with a Wissel (Wissenschaftliche Elektronik GmbH, Germany) electromechanical spectrometer working in a constant acceleration mode. A $^{57}\text{Co/Rh}$ (activity $\cong 50$ mCi) source and $\alpha\text{-Fe}$ standard were used. The experimentally obtained spectra were fitted using CONFIT2000 software [23]. The parameters of hyperfine interaction such as isomer shift (δ), quadrupole splitting (ΔE_q), effective internal magnetic field (B), line widths (Γ_{exp}), and relative weight (G) of the partial components in the spectra were determined.

2.3. Catalytic experiments

The water-gas shift activity tests were carried out in a flow reactor at atmospheric pressure. The catalytic measurements were conducted at the temperature range of $140\text{--}300^\circ\text{C}$. The applied experimental conditions were as follows: catalyst bed volume – 0.5 cm^3 , space velocity – 4000 h^{-1} and the reactant feed with model gas mixture (3.76 vol.% CO , 25.01 vol.% H_2O and 71.23 vol.% Ar). Before catalytic tests the samples were submitted to controlled mild reduction in a reaction mixture (CO/Ar and water vapor) up to 300°C . The catalytic activity data were expressed by degree of CO conversion. The measurements were recorded after establishing of the steady-state conditions of conversion at corresponding temperatures.

3. RESULTS AND DISCUSSION

XRD patterns and calculated structural parameters of synthesized $\text{Au/Cu}_{1-x}\text{Mn}_x\text{Fe}_2\text{O}_4$ samples are presented in Figure 1 and Table 1. Spinel ferrite phase and gold phase were proved in all synthesized samples. In copper-rich composition additional phase of CuO was present. Simultaneous presence of spinel phases with cubic (S.G.: Fd-3m , No. 227) and tetragonal (S.G.: $\text{I4}_1/\text{amd}$, No. 141) symmetry was found in $\text{Au/CuFe}_2\text{O}_4$, while even small substitution with manganese stabilize the cubic spinel phase. Average crystallite size of the cubic spinel phase was determined in the range $18\text{--}58\text{ nm}$, as the size increases with increasing copper content. It could be noted that calculated lattice parameters are lower than expected. For example, calculated lattice

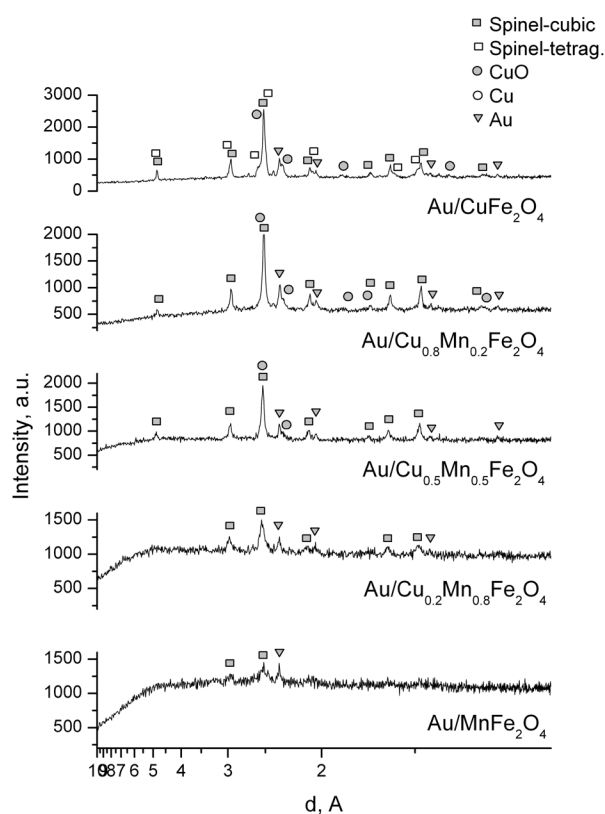


Fig. 1. X-ray diffraction patterns of Au/Cu_{1-x}Mn_xFe₂O₄ samples.

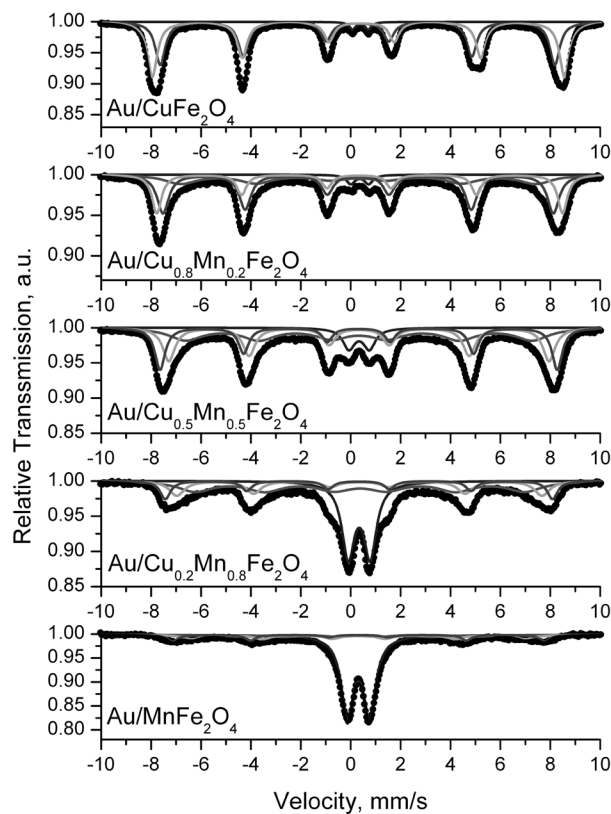


Fig. 2. Mössbauer spectra of Au/Cu_{1-x}Mn_xFe₂O₄ samples.

parameter of cubic spinel phase in Au/CuFe₂O₄ is 8.35 Å but standard parameter for CuFe₂O₄ is 8.37 Å. Because of that and presence of copper oxide phase found in the sample it can be concluded that the spinel phase is Cu-deficient and could be presented as Cu_(1-y)Fe_(2+y)O₄.

Mössbauer spectra and fitted parameters are presented in Figure 2 and Table 2. Spectra were fitted with model consisting of two or three sextets and one doublet. The sextets with lower values of isomer shift (Sx1) correspond to tetrahedrally coordinated Fe³⁺ in spinel lattice. The sextets named Sx2 have higher isomer shift than Sx2 and are related to Fe³⁺ in octahedral positions. Calculated hyperfine parameters of sextets in spectrum of Au/CuFe₂O₄ sample are typical for CuFe₂O₄ phase [9]. For the best fitting of spectra of Mn-containing samples a model with one additional sextet (Sx3) with lower values for hyperfine field and large line widths was used. The presence of this sextet could be explained with different number of tetrahedral Fe³⁺ near neighbours of octahedral Fe³⁺ accomplishing superexchange interactions. Therefore, part of Mn²⁺ and/or Cu²⁺ ions occupy tetrahedral positions in spinel lattice. It could be suggested that these ions are mainly Mn²⁺, because of the fact that quantity of

iron ions occupying tetrahedral positions decreases with increasing of Mn substitution. The doublet components in the spectra could be related to finely dispersed spinel particles with superparamagnetic behaviour.

The samples were also characterized after catalytic test in WGS. XRD patterns and calculated structural parameters are presented in Figure 3 and Table 1. The presence of cubic spinel phase and metallic copper and/or gold phases was established. Mössbauer analysis of these samples (Fig. 4, Table 2) evidenced changes in the ferrite phase. As it is seen in Table 2 isomer shift of the sextets related to octahedral iron ions increased compare to the values before catalytic test. This observation is an evidence for decreasing of the oxidation state of iron ions in octahedral coordination. The values of isomer shift are typical for magnetite where half of iron ions octahedral positions are in 2+ state and fast electron exchange with octahedral Fe³⁺ is realized. The presence of more than one sextet in spectra related to octahedral iron is due to small particles sizes and substituting elements of Cu and Mn in the spinel lattice. Obtaining of Cu- and/or Mn-substituted magnetite after WGS is confirmed by increasing of lattice parameters of spinel phase after WGS (Table 1).

Table 1. Average crystallites size (D) and lattice parameters of the crystalline phases in Au/Cu_{1-x}Mn_xFe₂O₄ samples after thermal treatment at 300 °C and after WGSR determined from the experimental XRD profiles

Sample	Phase	D, nm	Lattice parameters, Å	%
Au/CuFe ₂ O ₄	Spinel, cubic	57.7	a = 8.35	40
	Spinel, tetrag.	21.7	a = 5.83 c = 8.61	41
	Au	25.2	a = 4.08	1
	CuO	19.9	a = 4.67 b = 3.45 c = 5.11 beta = 99.55	18
Au/Cu _{0.8} Mn _{0.2} Fe ₂ O ₄	Spinel, cubic	26.3	a = 8.37	80
	Au	29.9	a = 4.08	1
	CuO	12.5	a = 4.68 b = 3.46 c = 5.13 beta = 99.96	19
Au/Cu _{0.5} Mn _{0.5} Fe ₂ O ₄	Spinel, cubic	24.1	a = 8.38	88
	Au	29.7	a = 4.07	1
	CuO	13.0	a = 4.68 b = 3.43 c = 5.07 beta = 99.42	11
Au/Cu _{0.2} Mn _{0.8} Fe ₂ O ₄	Spinel, cubic	18.4	a = 8.38	98
	Au	14.6	a = 4.07	2
Au/MnFe ₂ O ₄	Spinel, cubic	18.4	a = 8.38	98
	Au	21.7	a = 4.08	2
Au/CuFe ₂ O ₄ WGSR	Spinel, cubic	64.1	a = 8.40	77
	Cu	55.9	a = 3.61	23
Au/Cu _{0.8} Mn _{0.2} Fe ₂ O ₄ WGSR	Spinel, cubic	39.4	a = 8.42	84
	Au	16.2	a = 4.04	1
	Cu	33.6	a = 3.62	15
Au/Cu _{0.5} Mn _{0.5} Fe ₂ O ₄ WGSR	Spinel, cubic	37.3	a = 8.47	91
	Au	11.9	a = 4.03	1
	Cu	10.7	a = 3.63	8
Au/Cu _{0.2} Mn _{0.8} Fe ₂ O ₄ WGSR	Spinel, cubic	33.8	a = 8.50	95
	Au	12.1	a = 4.03	1
	Cu	11.9	a = 3.64	4
Au/MnFe ₂ O ₄ WGSR	Spinel, cubic	18.7	a = 8.49	99
	Au	25.5	a = 4.08	1

For better visualization of the changes of metallic phases during the catalytic reaction a graph with lattice parameters is presented in Figure 5. The calculated lattice parameters of gold and copper before and after catalytic tests and standard parameters according to PDF 4-784 and PDF 4-836 for gold and copper, respectively, are reported. The *a* parameter of gold in fresh samples is equal or nearly equal to the standard. In the XRD pattern of Au/CuFe₂O₄ sample after WGSR diffraction lines of gold were not observed, while *a* parameter of gold in sample Au/MnFe₂O₄ remained unchanged during reaction.

The lattice parameters of gold supported on mixed copper-manganese ferrites decreased after WGSR. This experimental result could be explained with copper incorporation in gold phase i.e. Au_{1-x}Cu_x alloy formation.

The temperature dependence of the degree of CO conversion during the WGSR over modified by gold copper and/or manganese ferrites is shown in Figure 6. The catalytic measurements revealed considerable differences in the catalysts activity. The following order was registered: Au/Cu_{0.2}Mn_{0.8}Fe₂O₄ ≥ Au/Cu_{0.5}Mn_{0.5}Fe₂O₄ > Au/Cu_{0.8}Mn_{0.2}Fe₂O₄ > Au/

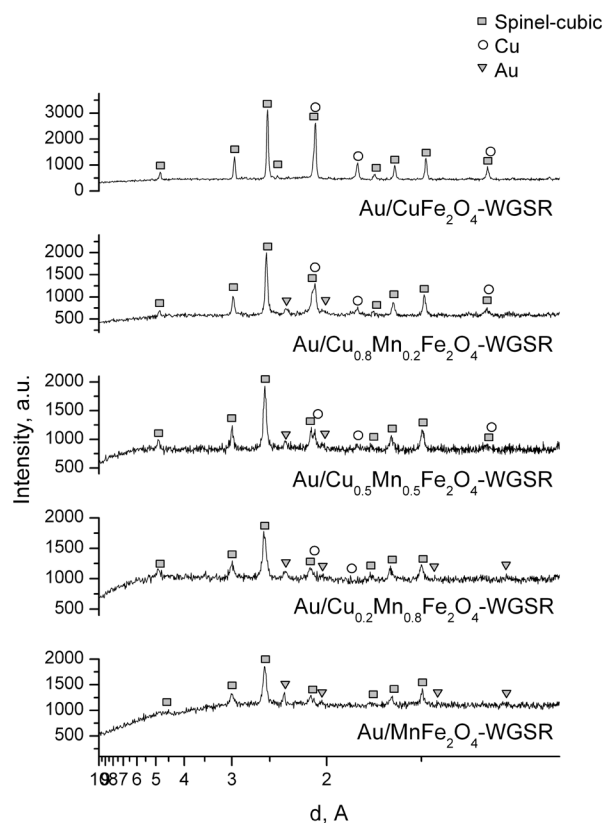


Fig. 3. X-ray diffraction patterns of Au/Cu_{1-x}Mn_xFe₂O₄ samples after WGSR.

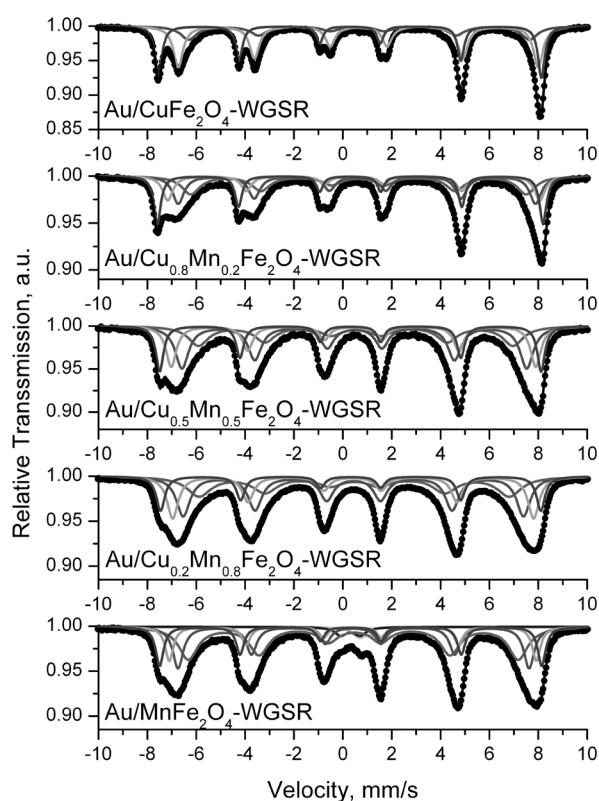


Fig. 4. Mössbauer spectra of Au/Cu_{1-x}Mn_xFe₂O₄ samples after WGSR.

CuFe₂O₄ ≥ Au/MnFe₂O₄. A strong synergetic effect between copper and manganese ions was observed. The CO conversion degree at 220 °C was more than 30% higher over the samples containing mixed copper-manganese ferrites in comparison with mono-component ones. The best performance above 220 °C exhibited Au/Cu_{0.2}Mn_{0.8}Fe₂O₄. Detailed structural characterization of the samples before and after catalytic tests allowed explaining the registered trend in the WGS activity. The main phase transformation after catalyst activation concerned the reduction of ferrite phase. According to XRD analysis, metallic copper phase and Cu and/or Mn substituted magnetite were formed in mixed copper-manganese formulations under reductive atmosphere. The simultaneous presence of these two phases could be considered as responsible for better WGS activity of the samples. The composition of mixed copper-manganese ferrites affected beneficially the formation of highly dispersed metallic copper particles. As reported in Table 1, the copper crystallites average size in mixed ferrites was significantly lower (between 10.7 and 33.6 nm) in comparison with those in Au/CuFe₂O₄ (55.9 nm). Additionally, analysing the role of gold modifica-

tion, it could be also suggested its effect on phase transformation. In both samples with lower copper content, i.e. the most active Au/Cu_{0.2}Mn_{0.8}Fe₂O₄ and Au/Cu_{0.5}Mn_{0.5}Fe₂O₄ with close activity in the low-temperature range up to 230 °C, metallic gold and copper particles with very similar sizes were found. In these cases the contribution of gold on spinel decomposition and highly dispersed copper particles stabilization could be hypothesized. The lower average size of spinel particles in these samples should be also mentioned. In agreement with data, reported in Figure 5, the modification by gold of the samples with higher amount of copper, i.e. Au/Cu_{0.8}Mn_{0.2}Fe₂O₄ and Au/CuFe₂O₄, obviously favoured alloying of gold and copper particles. The relatively higher size of copper crystallites and missing reflections of gold in XRD patterns of Au/CuFe₂O₄ allowed assuming of Au_{1-x}Cu_x alloy formation. This phenomenon affected negatively WGS activity by two reasons. The first one is related to the well-established ability of gold nanoparticles to activate CO molecules on their low coordination sites [24]. The second one concerns water dissociation that is a crucial step in the WGS reaction mechanism. Zhao et al. have reported

Table 2. Mössbauer parameters of investigated samples (δ – isomer shift, ΔE_q – quadrupole splitting, B – effective internal magnetic field, B_{mean} – mean effective internal magnetic field, Γ_{exp} – line widths, G – relative weight of the partial components in the spectra)

Sample	Components	δ , mm/s	ΔE_q , mm/s	B, T	Γ_{exp} , mm/s	G, %
Au/CuFe ₂ O ₄	Sx1 – Fe–tetra	0.28	0.00	49.1	0.48	46
	Sx2 – Fe–octa	0.37	–0.13	51.3	0.47	52
	Db – Fe ³⁺	0.39	0.63	–	0.29	2
Au/Cu _{0.8} Mn _{0.2} Fe ₂ O ₄	Sx1 – Fe–tetra	0.30	0.00	48.6	0.56	43
	Sx2 – Fe–octa	0.35	0.03	50.5	0.46	27
	Sx3 – Fe–octa	0.32	–0.02	44.2	1.57	27
	Db – Fe ³⁺	0.36	0.72	–	0.40	3
Au/Cu _{0.5} Mn _{0.5} Fe ₂ O ₄	Sx1 – Fe–tetra	0.32	0.00	49.4	0.49	27
	Sx2 – Fe–octa	0.34	–0.01	47.3	0.59	31
	Sx3 – Fe–octa	0.33	–0.01	43.1	1.57	34
	Db – Fe ³⁺	0.34	0.82	–	0.58	8
Au/Cu _{0.2} Mn _{0.8} Fe ₂ O ₄	Sx1 – Fe–tetra	0.33	0.00	48.2	0.49	14
	Sx2 – Fe–octa	0.35	0.01	45.5	0.73	18
	Sx3 – Fe–octa	0.38	–0.01	41.1	1.65	35
	Db – Fe ³⁺	0.34	0.88	–	0.61	33
Au/MnFe ₂ O ₄	Sx1 – Fe–tetra	0.31	0.00	46.3	0.50	11
	Sx2 – Fe–octa	0.32	0.00	41.5	0.80	14
	Sx3 – Fe–octa	0.32	0.02	31.3	1.00	9
	Db – Fe ³⁺	0.31	0.90	–	0.58	66
Au/CuFe ₂ O ₄ WGSR	Sx1 – Fe–tetra, Fe ₃ O ₄	0.29	0.00	48.7	0.33	34
	Sx2 – Fe–octa, Fe ₃ O ₄	0.64	–0.02	45.8	0.47	44
	Sx3 – Fe–octa, Fe ₃ O ₄	0.63	0.07	43.3	0.79	22
Au/Cu _{0.8} Mn _{0.2} Fe ₂ O ₄ WGSR	Sx1 – Fe–tetra	0.30	0.00	49.0	0.34	25
	Sx2 – Fe–octa	0.46	–0.01	47.3	0.50	18
	Sx3 – Fe–octa	0.59	–0.03	45.4	0.56	28
	Sx4 – Fe–octa	0.63	0.02	42.6	0.90	29
Au/Cu _{0.5} Mn _{0.5} Fe ₂ O ₄ WGSR	Sx1 – Fe–tetra	0.31	0.00	48.5	0.37	19
	Sx2 – Fe–octa	0.43	0.01	46.3	0.51	22
	Sx3 – Fe–octa	0.48	–0.01	43.8	0.66	35
	Sx4 – Fe–octa	0.54	–0.01	40.0	0.99	24
Au/Cu _{0.2} Mn _{0.8} Fe ₂ O ₄ WGSR	Sx1 – Fe–tetra	0.32	0.00	48.3	0.41	15
	Sx2 – Fe–octa	0.41	0.03	45.9	0.55	24
	Sx3 – Fe–octa	0.44	–0.01	43.3	0.67	34
	Sx4 – Fe–octa	0.48	–0.03	39.4	1.19	27
Au/MnFe ₂ O ₄ WGSR	Sx1 – Fe–tetra	0.32	0.00	48.6	0.38	17
	Sx2 – Fe–octa	0.40	0.02	46.7	0.40	14
	Sx3 – Fe–octa	0.43	0.02	44.6	0.52	24
	Sx4 – Fe–octa	0.46	–0.05	41.9	0.94	38
	Db1 – Fe ³⁺	0.31	0.80	–	0.60	3
	Db2 – Fe ²⁺	1.08	0.78	–	0.67	4

photoemission and STM studies for the adsorption and dissociation of water on Ce-Au(111) alloys found that alloys exhibited a relatively low reactivity toward water [25]. In this sense, the formation of Au-Cu alloy particles could cause diminished ability for water activation and, consequently, decreased WGS activity.

4. CONCLUSIONS

Copper-manganese-iron samples with nominal compositions Cu_{1-x}Mn_xFe₂O₄, where x=0; 0.2; 0.4; 0.6; 0.8 and 1 were prepared by auto-combustion sol-gel method. The materials were modified by gold. Spinel ferrite phase and gold phase were es-

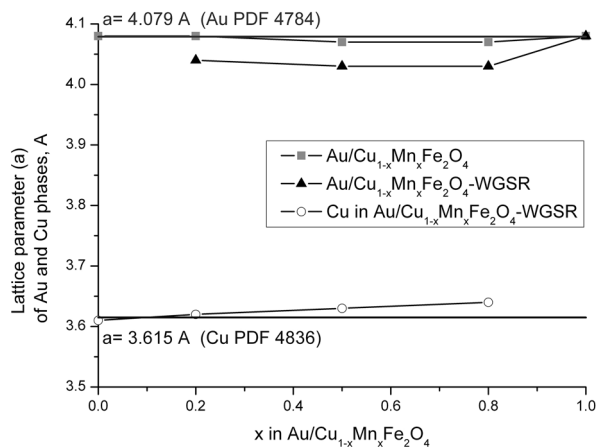


Fig. 5. Graphic of the calculated parameters.

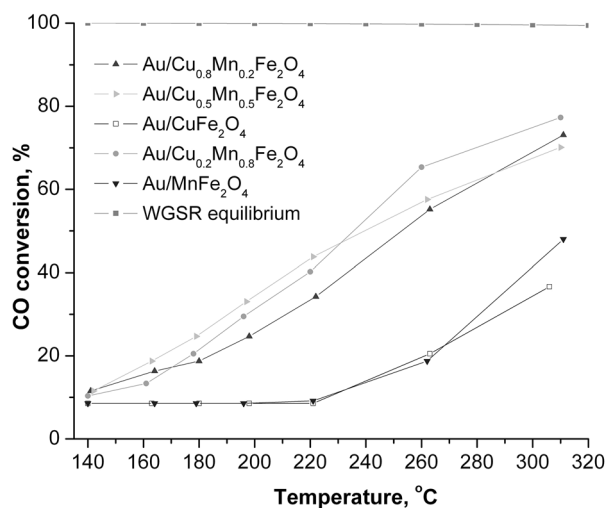


Fig. 6. Water-gas shift activity of Au/Cu_{1-x}Mn_xFe₂O₄ samples.

established in all synthesized samples. An increase of crystallite size of the cubic spinel phase was observed with increasing the copper content. The results of Mössbauer analysis showed that part of Mn²⁺ and/or Cu²⁺ ions occupy tetrahedral positions in spinel lattice and it could be suggested that these ions are mainly Mn²⁺. Partial reduction of iron ions in ferrite phase and formation of Cu, Mn-substituted magnetite was proved in samples after catalytic test. Reduction of the copper ions to metallic copper and formation of Au_{1-x}Cu_x alloy was evidenced, too. The role of the Cu-Mn ferrites composition on the WGS performance of gold-modified samples was studied and the following activity order was found: Au/Cu_{0.2}Mn_{0.8}Fe₂O₄ ≥ Au/Cu_{0.5}Mn_{0.5}Fe₂O₄ > Au/Cu_{0.8}Mn_{0.2}Fe₂O₄ > Au/CuFe₂O₄ ≥ Au/MnFe₂O₄. The variations in ferrites composition affected the WGS activity of the gold catalysts. A strong synergistic

effect was observed in mixed copper-manganese ferrites. This effect could be attributed to significant difference in the size of metallic copper and spinel particles formed under reaction conditions. The impact of gold on spinel transformation and highly dispersed copper particles stabilization was assumed.

Acknowledgements: T. Petrova and N. Velinov acknowledge financial support by the Bulgarian National Science Fund, Project DCOST 01/22/2017. I. Ivanov, T. Tabakova and V. Idakiev acknowledge financial support by the Bulgarian National Science Fund, Contract ДН 09/5/2016.

REFERENCES

1. P. V. Kovtunenkov, *Glass. Ceram.*, **54**, 143 (1997).
2. N. I. Velinov, T. M. Petrova, I. B. Ivanov, T. T. Tabakova, V. D. Idakiev, I. G. Mitov, *Hyperfine Interact.*, **238**, 72 (2017).
3. A. M. Wahba, M. B. Mohamed, *J. Magn. Magn. Mater.*, **378**, 246 (2015).
4. R. Tholkappian, K. Vishista, *Mater. Sci. Semicond. Process.*, **40**, 631 (2015).
5. K. Liu, A. I. Rykov, J. Wang, T. Zhang, *Adv. Catal.*, **58**, 1 (2015).
6. G. K. Reddy, P. G. Smirniotis, *Water Gas Shift Reaction—Research Developments and Applications*, Elsevier B.V, Amsterdam, 2015.
7. N. Velinov, K. Koleva, T. Tsoncheva, D. Paneva, E. Manova, K. Tenchev, B. Kunev, I. Genova, I. Mitov, *Cent. Eur. J. Chem.*, **12**, 250 (2014).
8. N. Velinov, K. Koleva, T. Tsoncheva, E. Manova, D. Paneva, K. Tenchev, B. Kunev, I. Mitov, *Catal. Commun.*, **32**, 41 (2013).
9. T. Tsoncheva, E. Manova, N. Velinov, D. Paneva, M. Popova, B. Kunev, K. Tenchev, I. Mitov, *Catal. Commun.*, **12**, 105 (2010).
10. N. Velinov, T. Petrova, I. Genova, I. Ivanov, T. Tsoncheva, V. Idakiev, B. Kunev, I. Mitov, *Mater. Res. Bull.*, **95**, 556 (2017).
11. L. L. Lang, J. Xu, Z. Z. Li, W. H. Qi, G. D. Tang, Z. F. Shang, X. Y. Zhang, L. Q. Wu, L. C. Xue, *Physica B*, **462**, 47 (2015).
12. A. Sutka, G. Mezinskis, *Front. Mater. Sci.*, **6**, 128 (2012).
13. H. Waqas, A. H. Qureshi, *J. Therm. Anal. Calorim.*, **98**, 355 (2009).
14. J. Azadmanjiri, S. A. SeyyedEbrahimi, H. K. Salehani, *Ceram. Int.*, **33**, 1623 (2007).
15. I. Szczygieł, K. Winiarska, *J. Therm. Anal. Calorim.*, **115**, 471 (2014).
16. J. Li, H. Yuan, G. Li, Y. Liu, J. Leng, *J. Magn. Magn. Mater.*, **322**, 3396 (2010).
17. S. Sam, A. Samson Nesaraj, *Int. J. Appl. Sci. Eng.*, **9**, 223 (2011).
18. K. Koleva, N. Velinov, T. Tsoncheva, I. Mitov,

- Hyperfine Interact.*, **226**, 89 (2014).
19. X. Lin, Y. Zhang, L. Yin, C. Chen, Y. Zhan, D. Li, *Int. J. Hydrogen Energy*, **39**, 6424 (2014).
 20. A. Khan, P. G. Smirniotis, *J. Mol. Catal. A: Chem.*, **280**, 43 (2008).
 21. D. Andreeva, V. Idakiev, T. Tabakova, A. Andreev, *J. Catal.*, **158**, 354 (1996).
 22. W. Kraus, G. Nolze, PowderCell for Windows, Federal Institute for Materials Research and Testing, Berlin, 2000.
 23. T. Žák, Y. Jirásková, *Surf. Interface Anal.*, **38**, 710 (2006).
 24. F. Boccuzzi, A. Chiorino, M. Manzoli, D. Andreeva, T. Tabakova, *J. Catal.*, **188**, 176 (1999).
 25. X. Zhao, S. Ma, J. Hrbek, J. A. Rodriguez, *J. Surf. Sci.*, **601**, 2445 (2007).